



Effect of granulocyte colony-stimulating factor on bone marrow: evaluation by intravoxel incoherent motion and dynamic contrast-enhanced magnetic resonance imaging

Fabio Minutoli¹ · Stefano Pergolizzi¹ · Alfredo Blandino¹ · Enricomaria Mormina² · Ernesto Amato¹ · Michele Gaeta¹

Received: 12 May 2019 / Accepted: 15 November 2019 / Published online: 10 December 2019
© Italian Society of Medical Radiology 2019

Abstract

Objective To report our experience with the use of intravoxel incoherent motion (IVIM) magnetic resonance imaging (MRI) and dynamic contrast-enhanced (DCE)-MRI in bone marrow before and after administration of granulocyte colony-stimulating factor (GCSF). Moreover, a small series of patients with bone metastases from breast cancer have been evaluated by IVIM DW-MRI and DCE-MRI before and after GCSF administration.

Materials and methods We studied with IVIM-MRI and DCE-MRI 14 patients with rectal or uterine cervix cancer studied before and 4–18 days after administration of GCSF; the second MR examination was obtained after three chemotherapy courses. IVIM perfusion fraction (f), pseudo-diffusion coefficient (D^*), true diffusion coefficient (D) and apparent diffusion coefficient (ADC) as well area under the curve at 60 s (AUC60) were calculated for bone marrow before and after GCSF administration. Moreover, two different IVIM parametric maps (i.e., ADC and ADC_{low}) were generated by selecting two different intervals of b values (0–1000 and 0–80, respectively). Furthermore, four patients affected by pelvic bone metastases from breast adenocarcinoma who received GCSF administration were also qualitatively evaluated for evidence of lesions on ADC maps, ADC_{low} maps and DCE-MRI.

Results ADC, D , D^* , f and AUC60 values were significantly higher in hyperplastic bone marrow than in untreated bone marrow (p values <0.0001 , <0.0001 , <0.001 , <0.001 , <0.0001 , respectively). All bone metastases were clearly differentiable from hyperplastic bone marrow on ADC_{low} maps, but not on ADC maps and DCE-MRI.

Conclusion MR functional imaging techniques, such as DW-, IVIM DW- and DCE-MRI are effective tools in assessing the response of bone marrow to the administration of growth factors. Although an overlap between signal of hyperplastic bone marrow and lytic bone metastases can occur on ADC maps and DCE-MRI, evaluation of ADC_{low} maps by IVIM DW-MRI could permit to differentiate hyperplastic bone marrow from lytic bone metastases. Further studies are needed to confirm our data.

Keywords Intravoxel incoherent motion · Diffusion-weighted imaging · Hyperplastic bone marrow · Granulocyte colony-stimulating factor

✉ Enricomaria Mormina
enricomaria.mormina@gmail.com

Fabio Minutoli
fminutoli@unime.it

Stefano Pergolizzi
stpergolizzi@unime.it

Alfredo Blandino
ablandino@unime.it

Ernesto Amato
eamato@unime.it

Michele Gaeta
michele.gaeta@unime.it

¹ Department of Biomedical and Dental Sciences
and of Morphofunctional Imaging, University of Messina,
Messina, Italy

² Department of Clinical and Experimental Medicine,
Policlinico Universitario “G. Martino”, University
of Messina, Via Consolare Valeria, 1, 98100 Messina, Italy

Introduction

Dynamic contrast-enhanced (DCE) and diffusion-weighted (DW) magnetic resonance imaging (MRI) are techniques of large interest owing to their ability to provide information on blood supply and cellularity in both normal and neoplastic tissues. Thus, they have been proposed as tools to detect cancer and to evaluate response to treatment [1–4]. Intravoxel incoherent motion (IVIM) DW-MRI is a method proposed by Le Bihan et al. to separate the signal arising from a diffusion sequence, such as the Stejskal and Tanner sequence, into a vascular and a nonvascular component [5, 6], allowing to estimate tissue diffusivity and tissue perfusion without using contrast medium [5, 7].

IVIM-based studies have shown that organs in the abdomen, including liver [8–10], pancreas [11] and kidneys [12], have relatively high fractional perfusion and pseudo-diffusion (i.e., fast component of diffusion) values compared with other organs, such as the brain [13, 14].

On the other hand, data about DW imaging of normal bone marrow and its changes after administration of hematopoietic growth factors such as granulocyte colony-stimulating factor (G-CSF) are limited [15, 16] and, to date, no study exists evaluating IVIM parameters in normal and hyperplastic bone marrow. The evaluation of IVIM DW imaging in such field seems to have a clinical relevance since G-CSF is increasingly used to reduce the neutropenia associated with chemotherapy [17] and it has been shown that on morphological MRI sequences, as well as on DW imaging and positron emission tomography (PET), G-CSF-induced bone marrow hyperplasia may hide metastatic bone lesions [15, 16, 18–23].

We evaluated the value of IVIM DW-MRI and DCE-MRI techniques in assessing the response of bone marrow to the administration of G-CSF. Moreover, a small series of patients with bone metastases from breast cancer have been evaluated by IVIM DW-MRI and DCE-MRI before and after G-CSF administration.

Materials and methods

The study was approved by our institutional review board committee. Informed consent was obtained from each patient before each examination.

Subjects

In order to evaluate G-CSF effect on bone marrow, we included in our study patients who had an MRI examination of the pelvis both before and after administration of G-CSF

according to the following inclusion criteria: (1) an MRI examination of the pelvis was performed for staging of rectal or uterine cancers, (2) a second pelvic MRI examination was obtained after chemotherapy no more than 3 months later, (3) the second MRI examination was obtained between 4 and 20 days after administration of G-CSF, (4) no evidence of bone metastases during 1 year follow-up.

According to the above reported inclusion criteria, fourteen consecutive patients (nine female, five male; age range 44–75 years; mean age 55 years) with locoregionally recurrent or locally advanced rectal or uterine cervix cancer were included. The second MRI examination was performed after three chemotherapy courses (using capecitabine and oxaliplatin in rectum cancer patients and fluorouracil, cisplatin and/or taxol in uterine cervix cancer patients) and between 4 and 18 days (median 9 days) after administration of G-CSF. All the included patients received 6 mg pegfilgrastim administered subcutaneously.

Additionally, as anecdotal example of the capability of IVIM DW imaging to differentiate hyperplastic bone marrow from bone metastases, we also evaluated, before and after G-CSF administration, twelve pure lytic or prevalently lytic metastases of the pelvic bones [as demonstrated on conventional X-ray films and/or computed tomography (CT)] in four additional patients (four female; age range 51–70 years, mean age 58 years) with breast adenocarcinoma. At time of the first MRI study, patients had not received previous treatment with chemotherapy, radiotherapy or bisphosphonates, whereas a second MRI examination was obtained after three chemotherapy courses (anthracycline and taxol) no more than 3 months later and 7–18 days (median 10 days) after administration of G-CSF.

Diagnosis of bone metastasis was made on the basis of clinical history (e.g., bone pain in patients with histologically proven cancer), and on one or more of the following diagnostic examinations: ^{99m}Tc -methylene diphosphonate bone scintigraphy, PET scan, conventional radiography, CT, bone marrow biopsy.

The diameter of pelvic bone metastases ranged from 1 up to 4 cm (mean diameter 2.8 cm). None of the considered metastases had undergone bone marrow biopsy.

MR imaging

All the MR examinations were performed with a 1.5-T scanner (Achieva; Philips Medical Systems, Best, the Netherlands) using a SENSE XL Torso coil with 16 elements in all the patients.

The following MRI sequences were used, covering the inferior abdomen from the sub-throcantheric regions up to the iliac crests: axial fast short tau inversion recovery (STIR) (repetition-time (TR), 4000 ms; echo time (TE), 50 ms; inversion-time, 140 ms; flip angle, 80°; slice thickness,

6 mm; matrix 314×314), axial T1-weighted dual-echo fast field echo (FFE) (TR, 300 ms; TE, 2.3/4.6 ms; flip angle, 80°; slice thickness, 6 mm; matrix 280×225), axial diffusion weighted (TR, 1880 ms; TE, 73 ms; slice thickness, 6 mm; matrix, 124×124; b values of 0, 20, 40, 80, 100, 600, 1000 s/mm²) with spectral pre-saturation inversion recovery (SPIR) fat saturation. The use of two b values lower than 50 s/mm² is mandatory to obtain reliable values of perfusion-sensitive IVIM parameters [23–25].

DCE examination was performed with a 3D spectral attenuated inversion recovery (SPAIR) T1-weighted high-resolution isotropic volume examination (e-THRIVE) sequence using the following parameters: TR, 4.4 ms; TE, 2.2 ms; flip angle, 10°; matrix, 180×180; acquisition time, 4–6 s. An automated power injector (Mallinckrodt, Hazelwood, MO, USA) was used to inject a bolus of 0.2 mL of gadoteratemeglumine (gadolinium concentration 0.5 mol/L) per kilogram of body weight through a catheter inserted into an antecubital vein at a rate of 3 mL/s, followed by a 30-mL saline at the same flow-rate. The sequence was started when half the contrast medium had been injected, performing 40 samples of the tissue.

Imaging post-processing and data analysis

Bone marrow intensity evaluation was performed by two radiologists working in consensus. Image analysis was performed at a multimodality workstation and all available MR images were reviewed. In each subject, three circular regions of interest (ROIs) with a size of 200, 300 and 480 mm² were manually placed on IVIM DW images and DCE images, using fast-STIR and T1-weighted MR images as references, respectively, in the following areas: (1) left femoral neck (200 mm²), (2) left iliac bone 2 cm above the acetabular roof (300 mm²), and (3) center of the first sacral vertebra (480 mm²). These areas represent the largest part of the three different pelvis bones with higher content of active red bone marrow in adults. Each measure was performed on images obtained both before and after treatment with GCSF by using the same ROI through a paste and copy tool and mean value was used to perform statistical analysis. To permit analysis of the images obtained at different time points, pre- and post-treatment images were coregistered using SPM8 toolbox coregister function by using full affine transformation with 12 degrees of freedom before ROIs were drawn.

To examine the individual contributions to the apparent diffusion changes of true molecular diffusion and incoherent motion of water molecules in the capillary network, perfusion fraction (f), perfusion-free diffusion coefficient (D) and pseudo-diffusion (D^*) were estimated using a least-square nonlinear fitting in MATLAB (MathWorks, Natick, MA) by fitting the DW signal decay in the ROIs to the IVIM bi-compartmental model as follows [5, 26]. The following

equation was employed to express the relationship between signal intensities at $b = 0$ (S_0) and at each b value (S_b):

$$S_b/S_0 = (1 - f_{\text{slow}}) \exp(-bD_{\text{fast}}) + f_{\text{slow}} \exp(-bD_{\text{slow}}) \quad (1)$$

where $(1 - f_{\text{slow}})$ represents the perfusion fraction f , D_{slow} the perfusion-free diffusion coefficient (i.e., slow component of diffusion) D , and D_{fast} is related to the pseudo-diffusion coefficient (i.e., fast component of diffusion) D^* as follows: $D_{\text{fast}} = D + D^*$. We determined f , D and D^* values by fitting experimental data by means of a Levenberg–Marquardt algorithm [27]. The global apparent diffusion coefficient (ADC) was then obtained according to Messiou et al. [23] by fitting all S_b data through the mono-exponential law:

$$S_b = S_0 \exp(-b \text{ADC}) \quad (2)$$

Moreover, two different IVIM parametric maps (i.e., ADC and ADC_{low}) were also generated by selecting two different intervals of b values (0–1000 and 0–80, respectively) [8, 28, 29] (Figs. 1e, f, 2g–i).

DCE-MRI data were calculated using a semiquantitative method, analyzing the area under the curve over the first 60 s (AUC60) [1–3].

Because of the small number of patients with bone metastases, only a qualitative analysis was performed; evaluation of IVIM DW- and DCE-MRI parameters in these patients and comparison with hyperplastic bone marrow were not performed. Two independent radiologists, using fast-STIR and T1-weighted MR images as references, visually analyzed ADC maps, ADC_{low} maps and DCE-MR images of patients with pelvic bone metastases who had received GCSF administration and defined the evidence of bone metastasis into four degrees as follows: (1) definitely not appreciable, (2) probably not appreciable, (3) probably appreciable and (4) definitely appreciable.

Statistical analysis

Continuous variables were expressed as mean (\pm SD). A Student's T test was conducted to compare the value of each parameter before and after the administration of the GCSF. Differences were considered significant if the P value was < 0.05 .

Statistical analyses were performed by using SPSS, version 15 (SPSS, Inc., Chicago, USA) software.

Results

The data obtained from bone marrow and hyperplastic bone marrow (i.e., after GCSF administration) are summarized in Table 1.

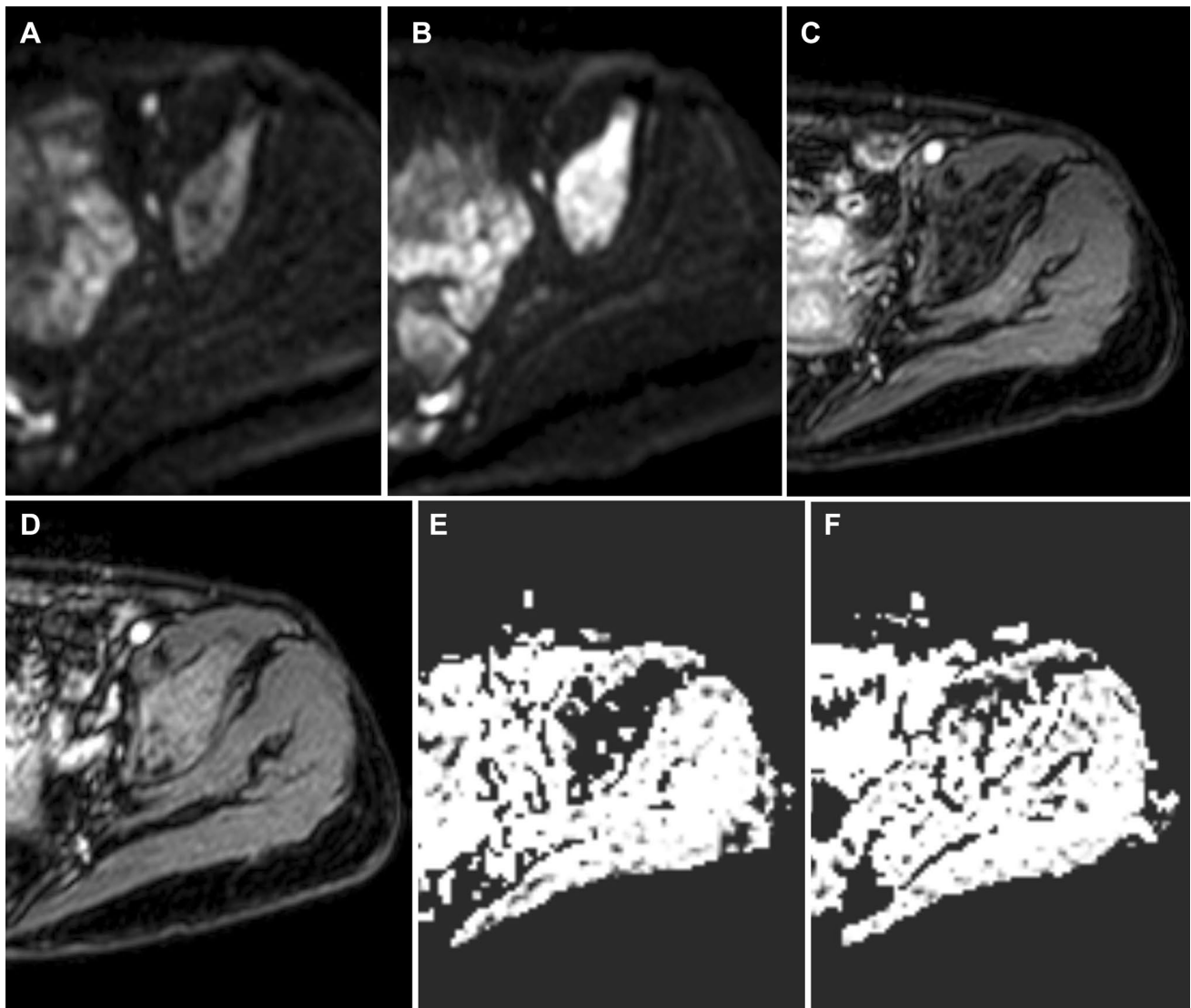


Fig. 1 Axial diffusion-weighted images ($b=1000$) of the left iliac bone marrow obtained before (a) and after (b) treatment with GCSF show an evident post-treatment increase in the signal, suggesting increased cellularity. Axial images obtained during arterial phase of dynamic gadolinium enhanced examination before (c) and after (d)

treatment with GCSF demonstrate an intense increase of enhancement of the hyperplastic bone marrow. The axial parametric ADC_{low} maps clearly demonstrate the difference of perfusion before (e), and after (f) treatment with GCSF showing an evident hyperintensity of hyperplastic bone marrow

A strong statistically significant difference between pre-treatment and post-treatment (i.e., after GCSF administration) bone marrow parameters was found for ADC ($P < 0.0001$), f ($P < 0.001$), D ($P < 0.0001$) and D^* ($P < 0.001$) IVIM parameters, representing an increase in cellularity and perfusion in hyperplastic bone marrow (Fig. 1a b, e, f). A statistically significant increase after GCSF stimulation was also found for AUC60 values (Fig. 1c, d) ($P < 0.0001$).

As far as bone metastases are concerned (Fig. 2), they were considered “definitely appreciable” (i.e., clearly distinguishable from hyperplastic bone marrow) on ADC_{low} maps (Fig. 2i) by both independent readers. On the other hand,

both readers, evaluating ADC maps and DCE-MR images, considered 25% of bone metastases “definitely not appreciable,” 25% “probably not appreciable,” 25% “probably appreciable” and 25% “definitely appreciable” (Fig. 2f, h).

Discussion

Our data validate IVIM imaging as a method to measure increased cellularity and perfusion in the bone marrow after administration of GCSF; namely, our data demonstrated that ADC, f , D^* , D and AUCG60 change under GCSF

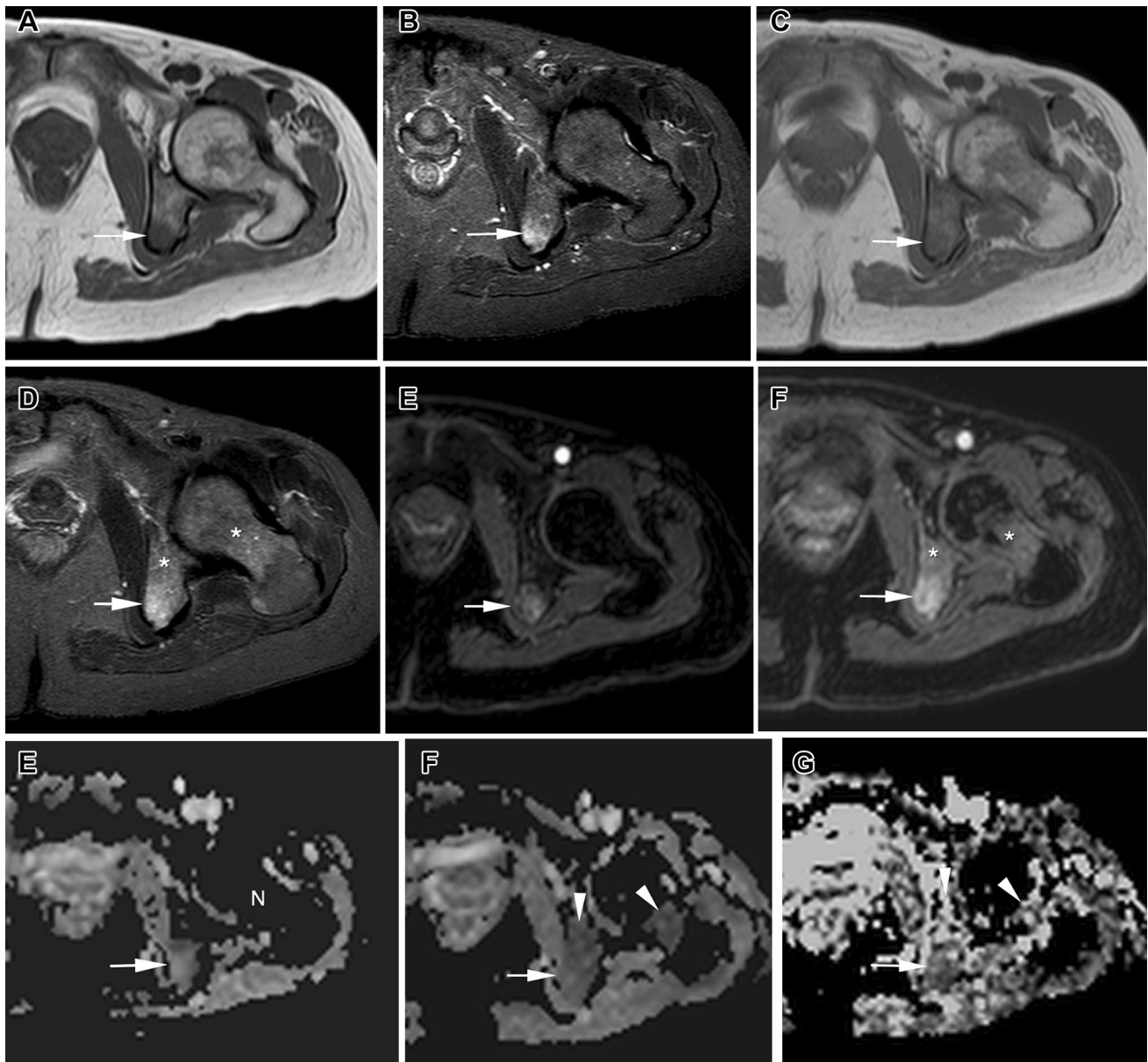


Fig. 2 66-year-old woman with bone metastasis from breast carcinoma. Axial T1-weighted (a) and fast-STIR (b) images through the left hip show a metastasis (arrow) which is masquerade by hyperplastic bone marrow (asterisks) after treatment with GCSF (c, d). On axial images obtained during arterial phase of dynamic gadolinium enhanced examination, the metastasis (arrow) is well depicted before treatment with GCSF (e), but is faintly distinguishable from hyper-

plastic bone marrow (asterisks) after treatment with GCSF (f). The lesion (arrow), which on ADC image through femoral neck (N), is easily visible before GCSF (g) but became isointense with respect to hyperplastic bone marrow (arrowheads) (h), appears hypointense (less vascularized) in comparison with hyperplastic bone marrow (arrowheads) on the ADC_{low} map (i)

stimulation. To our knowledge, this was not previously well established in other studies.

GCSF has a broad impact on hematopoiesis, stimulating the development and maturation of committed stem cells to neutrophils, eosinophils and monocytes [30] and, consequently, causing an increase in bone marrow cellularity. In addition, GCSF is a potent angiogenic which enhances capillary formation increasing the number of microvessels

in bone marrow [31]. As a result of the administration of GCSF, hyperplastic red marrow appears darker than normal on T1-weighted scans and may have a slightly increased signal intensity on T2-weighted and STIR sequences. In healthy individuals, GCSF application leads to significant signal changes of bone marrow in lumbar vertebrae that are maximal about 2 weeks after discontinuation of GCSF application [32]. These findings can be confused with bone

Table 1 IVIM mono-exponential quantitative parameter (ADC), IVIM biexponential quantitative parameters (D , D^* and f) and AUC60, of normal bone marrow before and after the administration of granulocyte colony-stimulating factor (GCSF)

Groups	ADC	D	D^*	f	AUC60
1. Bone marrow before GCSF	384 ± 62	210 ± 80	13,250 ± 1570	13.6 ± 2.2	26.1 ± 3.43
2. Bone marrow after GCSF	759 ± 86	540 ± 110	68,070 ± 14,500	22.7 ± 3.2	61.1 ± 3.85
p value (1 vs 2)	< 0.0001	< 0.0001	< 0.001	< 0.001	< 0.001

Values are reported as mean ± standard deviation. ADC, D and D^* values are expressed in units ($\mu\text{m}^2/\text{s}$); f is reported as percentage. AUC60 is reported in arbitrary units

metastases and infiltrative diseases of the marrow; on the other hand, bone metastases can become less conspicuous or “disappear” in patients receiving GCSF treatment [15, 18–22]. A similar phenomenon occurs also on PET scans because of increased metabolism of hyperplastic bone marrow [23].

Our data support the opinion that hyperplastic bone marrow can simulate bone metastases or can hide the presence of bone metastases not only on PET and morphological MRI scans but also on DW imaging [15, 18–23] which has recently emerged as an effective method to detect and monitor skeletal metastases [16] among other MR-based approaches (namely, chemical shift imaging, susceptibility weighted ($T2^*$) sequences and ultrashort echo time sequences) [15, 33, 34]. However, the use of ADC_{low} maps allows a reliable differentiation between hyperplastic bone marrow and breast cancer bone metastases.

Using b values 50/800–900, Padhani found a significant difference between ADC of normal red bone marrow (mean value 675 $\mu\text{m}^2/\text{s}$) and bone marrow involved by breast cancer metastases and myeloma (mean value 920 $\mu\text{m}^2/\text{s}$) and defined 774 $\mu\text{m}^2/\text{s}$ as the optimal ADC cutoff value for separating normal and malignant bone marrow. However, in 2 of 3 patients treated with CGSF, ADC values of hyperplastic bone marrow were similar to ADC values of metastases [21]. In our series, mean ADC value of hyperplastic bone marrow was 759 $\mu\text{m}^2/\text{s}$ (range 568–912), and an overlap between signal of hyperplastic bone marrow and bone metastases from breast carcinoma occurred on ADC maps (Fig. 2h). On the other hand, bone metastases were clearly depictable on ADC_{low} maps obtained after GCSF administration (Fig. 2i). Another interesting issue of our study regards the effect of increased vascularization of bone marrow induced by GCSF, which could be appreciated with DCE-MRI and could hide the presence of bone metastases (Fig. 2f). On the other hand, increased vascularization was responsible of strong increase of D^* (i.e., pseudo-diffusion) in hyperplastic bone marrow in comparison with normal bone marrow; furthermore, pseudo-diffusion of hyperplastic bone marrow was also higher than bone metastases one, as appreciable on ADC_{low} maps. Consequently, D^* could be a useful marker in distinguishing metastases from hyperplastic bone marrow.

The main limitation of our study is the fairly small cohort of patients with bone metastases that does not allow us to define the utility of ADC_{low} maps in the distinction between hyperplastic bone marrow and metastases with adequate statistical power. However, our data suggest the advisability that studies including a larger group of patients should be performed to confirm our results.

A second weakness could be the use of a semiquantitative parameter (AUC60) for the evaluation of DCE-MRI. Semiquantitative parameters may not accurately reflect contrast agent concentration in the tissue of interest and can be influenced by the contrast agent injection procedure and the scanner settings (including pulse sequence, gain and scaling factors). On the other hand, AUC60 has the advantage of being relatively straightforward to acquire, has been demonstrated to parallel parameters of vessel permeability obtained using more complex mathematical modeling [2], is a relatively robust kinetic parameter being able to characterize all enhancing regions without the problems associated with model fitting failures (namely in the case of highly vascularized regions, very poorly perfused regions or physiological motion) [35]; therefore, it has been recommended as a practical substitute for K -trans in clinical studies [36].

Moreover, the reproducibility of f and D^* estimations may be considered low [37]; however, we used two b values lower than 50 mm^2/s , according to a study of Cohen [24] who showed relatively high D^* repeatability when DW sequence includes two very low b values.

Finally, absence of histological correlations represents a further drawback of our work.

In conclusion, the main changes in the bone marrow after administration of growth factors are related not only to an increase in cellularity but also to an enhanced vascularization, as demonstrated by the increase in IVIM perfusion parameters (i.e., D^* and f) and of AUC60. Thus, MR functional imaging techniques, such as DW-, IVIM DW- and DCE-MRI, are effective tools in assessing the response of bone marrow to the administration of growth factors. Moreover, the use of IVIM DW-MRI could overcome diagnostic problems related to the presence of hyperplastic bone marrow, namely falsely positive diagnosis of metastatic bone involvement as well as false negative results due to

obscuration of bone metastases. Further studies including a higher number of patients and more precise imaging time points relative to GCSF administration are required to confirm our findings.

Compliance with ethical standards

Conflict of interest The authors declare that they have no conflict of interest.

Ethical standards All procedures performed in studies involving human participants were in accordance with the ethical standards of the institutional and/or national research committee and with the 1964 Helsinki declaration and its later amendments or comparable ethical standards.

Ethical approval The study was approved by our institutional review board committee.

Informed consent Informed consent was obtained from each patient before each examination.

References

- O'Connor JP, Jackson A, Parker GJ et al (2007) DCE-MRI biomarkers in the clinical evaluation of antiangiogenic and vascular disrupting agents. *Br J Cancer* 96:189–195
- Evelhoch JL (1999) Key factors in the acquisition of contrast kinetic data for oncology. *J Magn Reson Imaging* 10:254–259
- Li SP, Padhani AR, Makris SA (2011) Dynamic contrast-enhanced magnetic resonance imaging and blood oxygenation level-dependent magnetic resonance imaging for the assessment of changes in tumor biology with treatment. *J Natl Cancer Inst Monogr* 43:103–107
- Gaeta M, Benedetto C, Minutoli F et al (2014) Use of diffusion-weighted, intravoxel incoherent motion, and dynamic contrast-enhanced MR imaging in the assessment of response to radiotherapy of lytic bone metastases from breast cancer. *Acad Radiol* 21:1286–1293
- Le Bihan D, Breton E, Lallemand D et al (1988) Separation of diffusion and perfusion in intravoxel incoherent motion MR imaging. *Radiology* 168:497–505
- Stejskal EO, Tanner JE (1965) Spin diffusion measurements: spin echoes in the presence of a time-dependent field gradient. *J Chem Phys* 42:288–292
- Le Bihan D, Breton E, Lallemand D, Grenier P, Cabanis E, Laval-Jeantet M (1986) MR imaging of intra-voxel incoherent motions: application to diffusion and perfusion in neurologic disorders. *Radiology* 161:401–407
- Patel J, Sigmund EE, Rusinek H, Oei M, Babb JS, Taouli B (2010) Diagnosis of cirrhosis with intravoxel incoherent motion diffusion MRI and dynamic contrast-enhanced MRI alone and in combination: preliminary experience. *J Magn Reson Imaging* 31:589–600
- Luciani A, Vignaud A, Cavet M et al (2008) Liver cirrhosis: intravoxel incoherent motion MR imaging—pilot study. *Radiology* 249:891–899
- Chow AM, Gao DS, Fan SJ et al (2012) Liver fibrosis: an intravoxel incoherent motion (IVIM) study. *J Magn Reson Imaging* 36:159–167
- Lemke A, Laun FB, Klauss M et al (2009) Differentiation of pancreas carcinoma from healthy pancreatic tissue using multiple b-values: comparison of apparent diffusion coefficient and intravoxel incoherent motion derived parameters. *Invest Radiol* 44:769–775
- Ichikawa S, Motosugi U, Ichikawa T, Sano K, Morisaka H, Araki T (2013) Intravoxel incoherent motion imaging of the kidney: alterations in diffusion and perfusion in patients with renal dysfunction. *Magn Reson Imaging* 31:414–417
- Wirestam R, Borg M, Brockstedt S, Lindgren A, Holtas S, Stahlberg F (2001) Perfusion-related parameters in intravoxel incoherent motion MR imaging compared with CBV and CBF measured by dynamic susceptibility-contrast MR technique. *Acta Radiol* 42:123–128
- Federau C, Maeder P, O'Brien K, Browaeys P, Meuli R, Haggmann P (2012) Quantitative measurement of brain perfusion with intravoxel incoherent motion MR imaging. *Radiology* 265:874–881
- Padhani AR, Gogbashian A (2011) Bony metastases: assessing response to therapy with whole-body diffusion MRI. *Cancer Imaging* 11:S129–S145
- Wu LM, Gu HY, Zheng J et al (2011) Diagnostic value of whole-body magnetic resonance imaging for bone metastases: a systematic review and meta-analysis. *J Magn Reson Imaging* 34:128–135
- Hartman RP, Sundaram M, Okuno SH, Sim FH (2004) Effect of granulocyte-stimulating factors on marrow of adult patients with musculoskeletal malignancies: incidence and MRI findings. *AJR* 183:645–653
- Ballon D, Watts R, Dyke JP et al (2004) Imaging therapeutic response in human bone marrow using rapid whole-body MRI. *Magn Reson Med* 52:1234–1238
- Fletcher BD, Wall JE, Hanna SL (1993) Effect of hematopoietic growth factors on MR images of bone marrow in children undergoing chemotherapy. *Radiology* 189:745–751
- Padhani AR, Koh DM, Collins DJ (2011) Whole-body diffusion-weighted MR imaging in cancer: current status and research directions. *Radiology* 261:700–718
- Padhani AR, van Ree K, Collins DJ, D'Sa S, Makris SA (2013) Assessing the relation between bone marrow signal intensity and apparent diffusion coefficient in diffusion-weighted MRI. *AJR* 200:163–170
- Doot RK, Dunnwald LK, Schubert EK et al (2007) Dynamic and static approaches to quantifying 18F-FDG uptake for measuring cancer response to therapy, including the effect of granulocyte CSF. *J Nucl Med* 48:920–925
- Messiou C, Collins DJ, Morgan VA, De Souza NM (2011) Optimising diffusion weighted MRI for imaging metastatic and myeloma bone disease and assessing reproducibility. *Eur Radiol* 21:1713–1718
- Cohen AD, Schieke MC, Hohenwarter MD, Schmainda KM (2015) The effect of low *b*-values on the intravoxel incoherent motion derived pseudodiffusion parameter in liver. *Magn Reson Med* 73:306–311
- Takahara T, Kwee TC (2012) Low *b*-value diffusion-weighted imaging: emerging applications in the body. *J Magn Reson Imaging* 35:1266–1273
- Dijkstra H, Baron P, Kappert P, Oudkerk M, Sijens PE (2012) Effects of microperfusion in hepatic diffusion weighted imaging. *Eur Radiol* 22:891–899
- Gao Q, Srinivasan G, Magin RL, Zhou XJ (2011) Anomalous diffusion measured by a twice-refocused spin echo pulse sequence: analysis using fractional order calculus. *J Magn Reson Imaging* 33(5):1177–1183
- Koh DM, Collins DJ, Orton MR (2011) Intravoxel incoherent motion in body diffusion-weighted MRI: reality and challenges. *AJR* 196:1351–1361
- Li SP, Padhani AR (2012) Tumor response assessments with diffusion and perfusion MRI. *J Magn Reson Imaging* 35:745–763

30. Lieschke GJ, Burgess A (1992) Granulocyte colony-stimulating factor and granulocyte-macrophage colony-stimulating factor. *N Engl J Med* 327:28–35
31. Pelletier L, Regnard J, Fellmann D, Charbord P (2000) An in vitro model for the study of human bone marrow angiogenesis: role of hematopoietic cytokines. *Lab Invest* 80:501–511
32. Althoefer C, Bertz H, Ghanem NA, Langer M (2001) Extent and time course of morphological changes of bone marrow induced by granulocyte-colony stimulating factor as assessed by magnetic resonance imaging of healthy blood stem cell donors. *J Magn Reson Imaging* 14(2):141–146
33. Vanel D, Casadei R, Alberghini M, Razgallah M, Busacca M, Albisinni U (2009) MR imaging of bone metastases and choice of sequence: spin echo, in-phase gradient echo, diffusion, and contrast medium. *Semin Musculoskelet Radiol* 13:97–103
34. Messiou C, Collins DJ, Morgan VA et al (2010) Quantifying sclerotic bone metastases with 2D ultra short TE MRI: a feasibility study. *Cancer Biomark* 7:211–218
35. Zweifel M, Padhani AR (2010) Perfusion MRI in the early clinical development of antivasular drugs: decorations of decision making tools? *Eur J Nucl Med Mol Imaging* 37:S164–S182
36. Leach MO, Brindle KM, Evelhoch JL et al (2005) The assessment of antiangiogenic and antivasular therapies in early-stage clinical trials using magnetic resonance imaging: issues and recommendations. *Br J Cancer* 92:1599–1610
37. Andreou A, Koh DM, Collins DJ et al (2013) Measurement reproducibility of perfusion fraction and pseudodiffusion coefficient derived by intravoxel incoherent motion diffusion-weighted MR imaging in normal liver and metastases. *Eur Radiol* 23:428–434

Publisher's Note Springer Nature remains neutral with regard to jurisdictional claims in published maps and institutional affiliations.